Tyrosinase-induced neuromelanin accumulation triggers rapid dysregulation and degeneration of the mouse locus coeruleus

Alexa F. Iannitelli[1], Arielle Segal[1], Jean-Francoise Pare[3], Bernard Mulvey[2], L. Cameron Liles[1], Steven A. Sloan[1], Katharine E. McCann[1], Joseph D. Dougherty[2,4], Yoland Smith[3,5], David Weinshenker[1*]

[1]Department of Human Genetics, Emory University School of Medicine, Atlanta, GA 30322, USA

[2]Department of Genetics, Washington University School of Medicine, St. Louis, MO 63110, USA

[3]Emory National Primate Research Center, Emory University, Atlanta, GA 30329, USA

[4]Department of Psychiatry, Intellectual and Developmental Disabilities Research Center, Washington University School of Medicine, St. Louis, MO 63110, USA

[5]Department of Neurology, Emory University School of Medicine, Atlanta, GA 30322, USA

*Address correspondence to:

David Weinshenker, PhD

Department of Human Genetics

Emory University School of Medicine

615 Michael St., Whitehead 301

Phone: (404) 727-3106

Email: dweinsh@emory.edu

Abstract

Motor symptoms in Parkinson's disease (PD) are caused by degeneration of dopamine (DA) neurons of the substantia nigra (SN), while early non-motor symptoms such as anxiety and sleep disturbances are likely mediated by dysfunction of locus coeruleus (LC) norepinephrine (NE) neurons. The LC develops α-synuclein pathology prior to SN DA neurons in PD, and later undergoes degeneration, but the mechanisms responsible for its vulnerability are unknown. The SN and LC are the only structures in the brain that produces appreciable amounts of neuromelanin (NM), a dark cytoplasmic pigment. It has been proposed that NM initially plays a protective role by sequestering toxic catecholamine metabolites and heavy metals, but may become harmful during aging and PD as they overwhelm cellular machinery and are released during neurodegeneration. Rodents do not naturally produce NM, limiting the study of causal relationships between NM and PD-associated LC pathology. Adapting a viral-mediated approach for expression of human tyrosinase, the enzyme responsible for peripheral melanin production, we successfully promoted pigmentation in mouse LC neurons that recapitulates key features of endogenous NM found in primates, including eumelanin and pheomelanin, lipid droplets, and a double-membrane encasement. Pigment expression results in mild neurodegeneration, reduced NE levels, transcriptional changes, and novelty-induced anxiety phenotypes as early as 1-week post-injection. By 6-weeks, NM accumulation is associated with severe LC neurodegeneration and a robust neuroinflammatory response. These phenotypes are reminiscent of LC dysfunction in PD, validating this model for studying the consequences of pigment accumulation in the LC as it relates to neurodegenerative disease.

Introduction

Parkinson's disease (PD) is a common neurodegenerative condition affecting nearly one million Americans and over 10 million individuals worldwide (Marras et al., 2018). PD is pathologically characterized by α-synuclein protein aggregation and subsequent degeneration of specific populations of catecholamine neurons, most notoriously dopamine (DA) neurons in the substantia nigra (SN) and norepinephrine (NE) neurons in the locus coeruleus (LC). The consequences of losing SN-DA neurons are well understood, as their death directly results in the emergence of motor symptoms, such as rigidity and tremor, which constitute a clinical diagnosis. The first line treatment for PD is DA replacement therapy with the precursor levodopa (L-DOPA), which ameliorates motor symptoms. However, PD is also characterized by early non-motor symptoms such as REM Sleep Behavior Disorder (RBD) (Stiasny-Kolster et al., 2005), anxiety (Prediger et al., 2012), depression (Remy et al., 2005), and cognitive impairment (Chan-Palay, 1991; Vazey and Aston-Jones, 2012; Hinson et al., 2017; Li et al., 2019) which may be mediated, at least in part, by LC dysfunction and degeneration (Zweig et al., 1993). LC dysfunction is closely associated with these prodromal symptoms in clinical studies (Del Tredici and Braak, 2013), and experimental manipulations of the LC faithfully recapitulate non-motor symptoms in animal models (Mavridis et al., 1991; Srinivasan and Schmidt, 2003; Song et al., 2019; Iannitelli et al., 2022). Importantly, these non-motor symptoms are not reversed by L-DOPA, and there are no alternative treatments available. As such, these early, LC-associated, pre-motor symptoms are often reported by PD patients to be detrimental to quality of life and present serious obstacles for maintaining independence.

The specific factors that make catecholamine neurons vulnerable to α-synuclein pathology, dysfunction, and death in PD are not fully understood, although several likely contributors have been identified. One notable feature of LC neurons is the length of their processes. As the LC is the primary source of central norepinephrine (NE), it projects to virtually every other region of the brain (Foote et al., 1983), resulting in long, highly branched, unmyelinated axons. The LC neurons have intrinsic pacemaker activity, which leads to high levels of oxidative stress (Wang and Michaelis, 2010) and risk for mitochondrial dysfunction (Sanchez-Padilla et al., 2014), factors which are well-studied in relation to PD etiology (Nicholls, 2008; Surmeier et al., 2010). Additionally, these noradrenergic neurons harbor toxic NE metabolites, including DOPEGAL (Kang et al., 2020). Perhaps the most defining characteristic of these neurons, though, is their unique expression of a dark, cytoplasmic pigment called neuromelanin (NM).

NM is found exclusively in catecholaminergic cells of the SN and LC, the two neuronal populations that are selectively vulnerable in PD (Zecca et al., 2004; Zecca et al., 2008b). NM is a byproduct of catecholamine synthesis and metabolism, and studies suggest that the formation of NM granules likely results from an overabundance of catecholamines that cannot be sequestered into vesicles quickly enough in active neurons (Sulzer et al., 2000). In addition to catecholamine metabolites, these granules contain melanins such as eumelanin and pheomelanin (Bush et al., 2006), lipid droplets, protein aggregates (Sulzer et al., 2008), and heavy metals, most notably iron (Zecca et al., 2008b). Thus, it has been proposed that the primary function of NM is to bind and sequester these harmful compounds in the cytoplasm so that they do not harm the neurons (Zecca et al., 2003). However, because SN-DA and LC-NE neurons do not possess the machinery required to break down these granules, NM accumulates over time, visibly

darkening the pigmentation of these brain regions with age. Eventually, this buildup of NM within catecholamine neurons may exacerbate neurodegeneration in PD either by interfering with and overwhelming cellular machinery and/or via release of previously bound toxins as it breaks down during cell death. Indeed, LC neurons containing the highest amounts of NM are disproportionately lost during both normal aging and PD (Mann and Yates, 1983), and increased iron (Sasaki et al., 2006), zinc (Dexter et al., 1992), and copper (Pall et al., 1987) are evident in brain and CSF samples from PD patients, suggesting dysregulation of heavy-metal homeostasis.

Despite the clear link between NM and neurodegeneration in PD, establishing a causal relationship has been difficult because NM is not produced endogenously in rodents, which comprise the majority of animal models for studying PD (Barden and Levine, 1983). It is not clear why rats and mice do not produce NM. It could be due to fundamental neurobiological differences between primate and rodent catecholamine LC neurons, or it may reflect their comparatively short life span (~2 years). Indeed, one study did report trace amounts of NM in aged rats (DeMattei et al., 1986), and even humans do not express detectable amounts of NM in LC neurons until they are 3 years old (Mann and Yates, 1974). Thus, despite an ever-growing toolbox of mouse genetic technology that makes them ideal for investigating the molecular mechanisms of disease, *in vivo* studies on NM have been extremely limited. To date, only two rodent models of NM has been reported (Zecca et al., 2008a; Carballo-Carbajal et al., 2019). The first study in rodents relied on purification and injection of human neuromelanin granules (Zecca et al., 2008a), but more recently, researchers were able to drive pigmentation in the SN of mice and rats through viral-mediated expression of human Tyrosinase (hTyr), the biosynthetic enzyme responsible for melanin production in the skin (Carballo-Carbajal et al., 2019). In this model, NM expression in the SN resulted in neurodegeneration and subsequent motor impairments

similar to those seen in other mouse models of PD. We have adapted this strategy to promote NM production in the mouse LC, developing the first rodent model of pigment expression in noradrenergic neurons. Here we present the characterization of this novel mouse model of PD through immunohistochemical and behavioral analyses, revealing neuroinflammatory and neurodegenerative responses coupled with a behavioral phenotype reminiscent of the non-motor features of PD. Additionally, we employed the Translating Ribosome Affinity Purification (TRAP) technique to enrich and sequence mRNA from these pigmented LC neurons, yielding insight into the molecular mechanisms of NM-mediated adaptations and neurotoxicity in the LC.

Materials and Methods

Animals. Adult male and female mice were used for all behavioral and immunohistochemical experiments. For immunohistochemistry, behavior, and HPLC, TH-Cre mice (B6.Cg-7630403G23RikTg(Th-cre)1Tmd/J, The Jackson Laboratory, # 008601) were used for the specific expression of Cre-dependent viral vectors in the LC. For translating ribosome affinity purification (TRAP) RNA-sequencing experiments, we crossed TH-Cre mice with transgenic *Slc6a2-eGFP*/*Rpl10a* mice (B6;FVB-Tg(*Slc6a2-eGFP*/*Rpl10a*)JD1538Htz/J, The Jackson Laboratory, #031151), which incorporate an EGFP/Rpl10a ribosomal fusion protein into a bacterial artificial chromosome under the *Slc6a2* (NE transporter; NET) promoter to allow for the isolation of polysomes and translating mRNAs specifically from noradrenergic neurons (Mulvey et al., 2018). Mice were group housed with sex- and age-matched conspecifics (maximum of 5 animals per cage) until one week prior to behavioral testing, and then individually housed for the subsequent week of experimentation until sacrifice. Animals were maintained on a 12:12 light:dark cycle (lights on at 0700), and food and water were available *ad*

libitum, unless otherwise specified. All experiments were conducted at Emory University in accordance with the National Institutes of Health *Guideline for the Care and Use of Laboratory Animals* and approved by the Emory Institutional Animal Care and Use Committee.

Viral vectors. To express hTyr in the LC, we developed an AAV5-EF1a-DIO-hTyr construct with assistance from the Emory Custom Cloning and Viral Vector Cores. For some preliminary experiments (immunohistochemistry for viral confirmation and gliosis, stereology), all mice were injected with AAV5-DIO-hTyr, and TH-Cre+ animals were used as the experimental group while TH-Cre- littermates served as the controls. For the remaining experiments (behavior, TRAP, and HPLC), only TH-Cre+ mice were used, and mice were injected with either the AAV5-DIO-hTyr experimental virus or a comparable AAV5-DIO-EYFP control virus (Addgene, plasmid #27056). Due to the volume of virus required for these experiments, several batches of AAV5-DIO-hTyr were produced. Despite our best efforts to control for titer and delivery, inherent variability was evident between batches. For this reason, some of the time courses varied between experiments. We are specific in our language characterizing the timeline of each individual experiment. For the purposes of consistency, the 1-2 week cohorts represent a time when NM is expressed by the LC, but has not led to widespread cell body death, while a 6-8 week cohort is used to illustrate considerable LC degeneration. The 4-week cohort presented in the discussion of astrocytic responding of the LC should be considered a mid-point of LC pigment accumulation.

Stereotaxic injections. Stereotaxic infusions were be performed as previously described (Tillage et al., 2020a), in a stereotaxic frame under 2.0% isoflurane anesthesia. Bilateral LC infusions were made at a volume of 0.5 μL/hemisphere using a 5 μL Hamilton glass syringe. The virus was

infused at a rate of 0.15 μL/min, and the needle was allowed to remain in place for 5 min following the completion of each infusion. LC coordinates are AP: - 5.4mm, ML: +/- 1.2mm, and DV: -4.0mm relative to Bregma.

High Performance Liquid Chromatography (HPLC). Mice were anesthetized with isoflurane and euthanized by rapid decapitation. The pons, prefrontal cortex, and hippocampus were rapidly dissected on ice and flash-frozen in isopentane (2-Methylbutane) on dry ice. The samples were weighed and stored at -80°C until processing for HPLC by the Emory HPLC Bioanalytical Core. As previously described (Lustberg et al., 2022), tissue was thawed on ice and sonicated in 0.1 N perchloric acid (10 μl/mg tissue) for 12 s with 0.5 s pulses. Sonicated samples were centrifuged (16,100 rcf) for 30 min at 4 °C, and the supernatant was then centrifuged through 0.45 μm filters at 4000 rcf for 10 min at 4 °C. For HPLC, an ESA 5600A CoulArray detection system, equipped with an ESA Model 584 pump and an ESA 542 refrigerated autosampler was used. Separations were performed using an MD-150 × 3.2 mm C18, 3 μm column (Thermo Scientific) at 30 °C. The mobile phase consisted of 8% acetonitrile, 75 mM NaH2PO4, 1.7 mM 1-octanesulfonic acid sodium and 0.025% trimethylamine at pH 2.9. A 20 μL of sample was injected. The samples were eluted isocratically at 0.4 mL/min and detected using a 6210 electrochemical cell (ESA, Bedford, MA) equipped with 5020 guard cell. Guard cell potential was set at 475 mV, while analytical cell potentials were −175, 100, 350 and 425 mV. The analytes were identified by the matching criteria of retention time measures to known standards (Sigma Chemical Co., St. Louis MO). Compounds were quantified by comparing peak areas to those of standards on the dominant sensor.

Immunohistochemistry. Mice were euthanized with an overdose of sodium pentobarbital (Fatal Plus, 150 mg/kg, i.p.; Med-Vet International, Mettawa, IL) and were transcardially perfused with cold 4% PFA in 0.01 M PBS for light microscopy and 4% PFA + 0.1% glutaraldehyde for electron microscopy. After extraction, brains were post-fixed overnight in 4% PFA at 4°C and then transferred to a 30% sucrose/PBS solution for 72 h at 4°C. Brains were embedded in OCT medium (Tissue-Tek) and sectioned by cryostat into 40-um-thick coronal sections at the level of the LC, anterior cingulate cortex (ACC), and hippocampus. Sections were blocked in 5% normal goat serum (NGS) in 0.01 M PBS/0.1% Triton-X permeabilization buffer and then incubated for 24 h at 4°C in NGS blocking buffer with primary antibodies listed in **Table 1**. Following washes in 0.01 M PBS, sections were incubated for 2 h in blocking buffer including secondary antibodies listed in **Table 1**. After washing, sections were mounted onto Superfrost Plus slides and cover-slipped with Fluoromount-G plus DAPI (Southern Biotech, Birmingham, AL).

Fluorescence Microscopy. For the catecholaminergic marker tyrosine hydroxylase (TH) and hTyr, immunofluorescent micrographs were acquired on a Leica DM6000B epifluorescent upright microscope at 20x magnification with uniform exposure parameters for each stain and region imaged. Brightfield images of pigment granules were also obtained on the Leica DM6000B upright microscope at 20x magnification. Following convention, these images are oriented with the dorsal direction up and the ventral direction down. For astrocyte marker glial fibrillary acidic protein (GFAP) and LC terminal marker NE transporter (NET), listed in **Table 1**, immunofluorescent images were acquired as z-stack images (10 z-stacks; pitch: 0.1 µm) at 20x magnification and compressed on a Keyence BZ-X700 microscope system. One

representative atlas-matched section was selected from each animal. Image processing for all images was conducted using the FIJI/ImageJ software.

Electron microscopy. Electron microscopy experiments were conducted by the laboratory of Dr. Yoland Smith at the Emory National Primate Research Center. All brains prepared for electron microscopy were cut in 60 mm-thick coronal sections with a vibrating microtome. Sections that included the locus coeruleus were rinsed in Phosphate buffer (PB; 0.1 M, pH 7.4) and then treated with 0.5% osmium tetroxide (OsO4) for 10 min (RT) and returned to PB. Sections were then dehydrated with increasing concentrations of ethanol; 1% uranyl acetate was added to the 70% ethanol solution to increase EM contrast (10 min incubation at RT in the dark). Sections were next placed in propylene oxide, followed by tissue embedding with an epoxy resin (Durcupan, Fluka) for at least 12 hr. Resin-embedded sections were then baked at 60°C for at least 48-hr until fully cured. Blocks containing the LC were removed before being cut into ultrathin 60 nm sections (Leica Ultracut T2). These ultrathin sections were mounted onto pioloform-coated grids and stained with lead citrate (5 min, RT) for added contrast. Grids were then examined with an electron microscope (EM; Jeol; Model 1011) coupled with a CCD camera (Gatan; Model 785) controlled with DigitalMicrograph software (Gatan; version 3.11.1).

For ultrastructual comparisons of hTyr-induced NM in mice and naturally produced NM in primates, three brainstem sections at the level of LC from a 16 year-old rhesus macaque were processed according to the same procedure and examined in the electron microscope.

Cell counts. TH-Cre+ animals received a unilateral LC injection of AAV5-DIO-hTyr in the right hemisphere. Coronal tissue sections were processed as described above (*Immunohistochemistry*)

and images were acquired as described for glial markers (*Fluorescence Microscopy*). Using TH as a guide for anatomical LC borders and DAPI as a marker for individual nuclei, sections were quantified using HALO imaging software (Indica Labs, v3.3.2541.420, FISH/IF v2.1.4). Nine sections were analyzed for each animal (n=4/group), covering most of the LC. The total area analyzed did not differ between the hTyr-injected hemisphere and the non-injected hemisphere. Within HALO, nuclei were defined using DAPI, and TH-positive and Nissl-positive nuclei cells were counted and summed across all nine sections for each animal. Comparisons were made between the number of Nissl+ and TH+ nuclei cells in the hTyr-injected hemisphere and the non-injected hemisphere.

Translating Ribosome Affinity Purification (TRAP). To obtain adequate quantities of RNA for sequencing, samples from two 6-8 month-old, same-sex and treatment TH-Cre+, *Slc6a2-eGFP*/*Rpl10a*+ mice were pooled to form a biological replicate by dissecting out the hindbrain posterior to the pontine/hypothalamic junction (cerebellum was discarded). Six biological replicates were collected per treatment group. Each replicate was homogenized and TRAP was performed as described (Mulvey et al., 2018; Iannitelli et al., 2022), resulting in LC-enriched "TRAP" samples and whole-hindbrain "input" samples. RNA was extracted using Zymo RNA Clean & Concentrator-5 kit, and subsequently sent for polyA-enriched library preparation and Illumina sequencing by NovoGene to a minimum depth of 20 million fragments per sample. Forward and reverse sequencing files from each replicate were aligned to the mouse genome (mm10) using STAR alignment, and counts were obtained using FeatureCounts in R Bioconductor. Two samples from saline-treated mice were removed from analysis because the TRAP protocol failed to enrich *Slc6a2* above a 10-fold change, a quality control threshold

observed in all other saline-treated samples. All subsequent analyses utilized R Bioconductor packages. Sequencing data are available on NCBI GEO (GSE226827).

To further characterize the gene expression changes, we performed analyses to compare gene expression patterns in our dataset with a repository of gene sets using Gene Set Enrichment Analysis (GSEA 4.2.3) (Mootha et al., 2003; Subramanian et al., 2005). Gene set permutation was used, as recommended by GSEA documentation for experiments with fewer than 7 samples per group. Other parameters were set to default settings using 1000 gene set permutations and signal to noise ranking metric. We downloaded KEGG Pathways from the Molecular Signatures Database, which has 186 gene sets. After filtering for the recommended minimum (15) and maximum (500) gene set size, the remaining 145 gene sets were compared to the expression data from our dataset to calculate the GSEA enrichment score and to compute significant enrichment.

Behavioral assays. Behavioral assays were performed in the following order, from least to most stressful.

Sleep latency: Latency to sleep was measured as the duration of time it took for the mouse to fall asleep following mild stimulation (gentle handling). A sleep bout was defined as 2 min of uninterrupted sleep behavior, followed by 75% of the following 8 min (Hunsley and Palmiter, 2004). This assay has been previously validated using EEG recordings (Porter-Stransky et al., 2019). Sleep testing began at 9:00 A.M., 2 h into the light cycle when mice typically engage in sleep behavior naturally. Videos were recorded for each session and scored by an experienced observer. Previous research by our group and other has revealed that increasing LC-NE

transmission decreases sleep latency, while NE depletion has the opposite effect (Porter-Stransky et al., 2019).

Novelty-suppressed feeding: Chow was removed from individual home cages 24 h prior to behavioral testing. Mice were moved to the test room under red light and allowed to habituate for 2 h prior to the start of the test. Individual mice were placed in a novel arena (10” × 18” × 10”) with a single pellet of standard mouse chow located in the center. The latency to feed, operationally defined as grasping and biting the food pellet, was recorded using a stopwatch. Mice that did not feed within the 15-min period were assigned a latency score of 900 s (Tillage et al., 2020b). We have shown that increasing NE promotes anxiety-like behavior in this task reflected by longer latencies to eat in the novel environment, while decreasing attenuates anxiety and reduces latency to eat (Lustberg et al., 2020c).

Fear conditioning and context testing: Fear-conditioning training and subsequent contextual fear testing is a widely used assessment of associative memory, particularly for an environment in which an aversive stimulus (footshock) was previously administered. This method has been described previously by our group and others and is sensitive to changes in NE (Murchison et al., 2004; Chalermpalanupap et al., 2018; Butkovich et al., 2020). Mice were placed in a fear-conditioning apparatus (7 in. x 7 in. x 12 in.; Coulbourn Instruments) with a metal shock grid floor. Following 3 min of habituation, three conditioned stimulus (CS)-unconditioned stimulus (US) pairings were presented with a 1-minute intertrial interval. The CS was a 20-second, 85 dB tone which co-terminated with the US, a 2-s, 0.5 mA footshock (Precision Animal Shocker, Colbour Instruments). The following day, the context test was conducted by placing animals back into the fear conditioning chamber without the administration of CS-US pairings. Freezing behavior was measured as a readout of memory for the fear-associated context.

Statistical analyses. Cell counting and HPLC measurements of catechol concentrations were compared between hTyr-injected and control groups using a student's t-test in GraphPad Prism. Similarly, behavioral assessment relied on t-test comparison between groups for latency to feed in the novelty-suppressed feeding task and average percent freezing in the contextual fear assay. R Bioconductor packages were utilized for statistical analyses of RNA sequencing data, including differential gene expression (DGE).

Results

Viral infusion of hTyr induces NM-like pigmentation in the LC of mice. To recapitulate NM found endogenously in the human LC, we adapted a viral vector-mediated approach to drive neuronal pigmentation in rodents. TH-Cre mice were stereotaxically infused with AAV5-DIO-hTyr in the LC to drive viral expression of hTyr (**Fig. 1a**), which is known to produce pigment when introduced in rodent SN DA neurons (Carballo-Carbajal et al., 2019). We found that hTyr expression likewise drove pigmentation of the LC in Cre+ (**Fig. 1b**) but not in Cre- mice (**Fig. 1c,d**) as early as 1 week post-infusion. This pigmentation was visible by gross anatomical inspection (**Fig. 1e**) and brightfield microscopy (**Fig. 1b**). Additionally, we confirmed the presence of melanin in this pigment using Fontana-Masson staining (**Fig. 1f**). We then utilized electron microscopy to compare the pigment granules in our rodent model (**Fig. 1g**) with endogenous NM granules from 16-year-old Rhesus macaque tissue (**Fig. 1h**). Ultrastructural inspection revealed that many of the components known to reside in endogenous NM, including pheomelanin and eumelanin pigments, lipid droplets, and a double membrane, were also present

in granules from our rodent model. Together, these results validate the use of hTyr expression to induce NM-like pigmentation in the mouse LC.

Pigmentation results in loss of LC fibers and cell bodies at 1-week. We next sought to determine if high levels of NM were protective or detrimental. Consistent with other rodent models of LC neurodegeneration (Chalermpalanupap et al., 2018; Butkovich et al., 2020), NET immunoreactivity, a marker of LC dendrite, axon, and terminal integrity, was visibly reduced in the LC (**Fig. 2a**), as well as in the LC projections to the anterior cingulate cortex (ACC) (**Fig. 2c**) and dentate gyrus (DG) (**Fig. 2d**) of hTyr-injected mice compared to EYFP-injected controls. To determine whether pigmentation impacted cell body integrity at 1 week post-injection, we performed a count of LC neurons. We quantified DAPI+ cells also positive for NeuroTrace Nissl in the LC in three mice per group, and found a 37% reduction of LC neurons in hTyr-injected mice compared to controls (**Fig. 2b**).

Pigmentation reduces NE levels throughout the LC network and dysregulates NE turnover in the projection fields at 1 week. Given the loss of LC axons/terminals, we assessed the impact of hTyr-driven pigmentation on tissue levels of catecholamines and their metabolites (**Fig. 3**) to determine if there was a loss of NE tone in target regions. NE was dramatically reduced in the pons, where LC cell bodies reside ($t_{(10)} = 10.14$, $p < 0.0001$), as well as in the prefrontal cortex (PFC; $t_{(10)} = 7.607$, $p < 0.0001$) and hippocampus ($t_{(10)} = 9.735$, $p < 0.0001$), two of the primary projection regions of the LC. Additionally, levels of the primary NE metabolite MHPG were also reduced in the pons ($t_{(10)} = 7.532$, $p < 0.0001$), PFC ($t_{(10)} = 5.152$, $p = 0.0004$) and hippocampus ($t_{(10)} = 3.666$, $p = 0.0043$) (**Fig. 3**). Despite the reduction of total NE and MHPG, the MHPG:NE

ratio, which provides an estimate of NE turnover, was significantly increased in the PFC ($t_{(10)}$ = 2.905, p = 0.0157) and hippocampus ($t_{(10)}$ = 4.392, p = 0.0014) compared to controls, suggesting adaptations in the LC-NE system (**Fig. 3**). Levels of other amine neuromodulators, including DA, 5-HT, and their respective metabolites, were unchanged with the exception of an increase in DA turnover (metabolite DOPAC:DA) in both the pons ($t_{(10)}$ = 3.288, p = 0.0082) and PFC ($t_{(10)}$ = 2.905, p = 0.0157), suggesting that dysfunction resulting from pigmentation of the LC was largely confined to the noradrenergic system at 1 week post-injection (**Table 2**).

The presence of LC pigment drives novelty-induced anxiety behavior at 1-week. Several prodromal symptoms of PD are regulated by the LC-NE system, and thus are sensitive to the early LC dysfunction which precedes neurodegeneration (Weinshenker, 2018). We assessed the impact of hTyr-induced pigmentation on LC-associated behaviors, including sleep, stress response, and cognition. We found hTyr-injected mice displayed a trend towards increased arousal, as measured by latency to fall asleep following gentle handling, compared to controls ($t_{(4)}$ = 2.414, p = 0.0732) (**Fig. 4a**). We found that hTyr-injected mice were significantly more reactive in a novelty-induced stress paradigm commonly used to model anxiety (Lustberg et al., 2020b). At 1 week post-injection, hTyr-expressing mice took significantly longer than EYFP controls to consume food in the novelty-suppressed feeding task ($t_{(24)}$ = 2.359, p = 0.0268) (**Fig. 4b**). Five hTyr-injected mice (approximately one third) timed out of the task at 15-min, while only one EYFP control mouse timed out of the task (**Fig. 4b**), further illustrating an increase in novelty-induced anxiety-like behavior resulting from LC pigmentation. Importantly, hTyr- and EYFP-injected mice displayed no differences in latency to eat in the home cage, indicating the experimental group's increased latency to eat during the task resulted from novelty stress

behavior rather than changes in satiety state. Associative memory, as measured by freezing in a footshock-associated context, did not differ between treatment groups (**Fig. 4c**).

hTyr-induced pigmentation alters LC transcriptome at 1-week. Next, we tested how the LC responded to the production of NM and subsequent adaptation using TRAP. Following confirmation of LC-mRNA enrichment with TRAP (**Fig. 5a**), we performed a gene set enrichment analysis (GSEA) to compare the gene expression patterns of our data with repositories of known gene sets. A volcano plot of differentially expressed genes is shown in **Fig. 5b**. We identified 10 KEGG pathways that were significantly enriched in the LC of hTyr-expressing animals, including Tyrosine metabolism (enrichment score (ES) = 0.622, p = 0.008), Tryptophan metabolism (ES = 0.596, p = 0.014), P53 stress signaling (ES = 0.513, p = 0.018), and lysosome activity (ES = 0.348, p = 0.042) (**Fig. 5c**).

Comparing our gene set to the Human Phenotype Ontology pathways, we found that hTyr samples displayed significant upregulation in the gene sets titled “Parkinsonism with favorable response to dopaminergic medication” (ES = 0.538, p = 0.039), “startle response” (ES = 0.558, p = 0.047), “speech articulation” (ES = 0.581, p = 0.04), and “sleep apnea” (ES = 0.591, p = 0.021) (**Fig. 5**).

The most significant transcriptional differences were seen when comparing our dataset to the Gene Ontology Biological Process gene sets. We found a staggering 140 gene sets significantly enriched in our hTyr group compared to EYFP controls. These pathways fell into four notable categories: apoptotic pathways, immune regulation, endoplasmic reticulum functioning, and heavy metal ion metabolism. Of these many upregulated pathways, we identified several that we predict are key regulators of NM-induced damage. Of particular

interest were the gene sets titled “antigen processing and presentation via MHC class I” (ES = 0.74, $p < 0.000$), “response to iron ion” (ES = 0.61, $p = 0.018$), “positive regulation of macroautophagy” (ES = 0.47, $p = 0.011$), and “pigment metabolic process” (ES = 0.46, $p = 0.024$) (**Fig. 5c**).

Finally, a comparison with the Gene Ontology Cell Component database showed 9 gene sets significantly enriched in the hTyr group compared to controls. The most notable was “pigment granule” (ES = 0.434, $p < 0.000$), with our rodent model displaying 45 core enriched genes of the 88 total present in the gene set (**Fig. 5c**).

Pigment accumulation results in neurodegeneration and neuroinflammation.

To assess the consequences of prolonged pigment burden in the LC, we allowed mice to age several weeks following viral infusion. Despite batch-dependent variability, we consistently saw a near-total loss of LC cell bodies by 6- to 8-weeks post-infusion, as measured by TH immunoreactivity (**Fig. 6**). Although only a few LC neurons remain at this time point, pigmented granules remained abundant in the region. In fact, pigment granules after 6-weeks (**Fig. 6**) were visibly darker and more robust than at 1-week (**Fig. 1**). By 6 weeks, the pigmentation was also visible beyond the confines of the LC. Taken together, these data suggest that pigmented granules persist following the death of their host neurons, and in fact may spread to adjacent tissue. Moreover, it appears that the most densely pigmented sub-regions of the LC display the most profound cell loss (**Fig. 7**), a finding which would mimic the patterns of neurodegeneration seen in human patients (Mann and Yates, 1983).

Glial cells help dispose of extracellular waste following neurodegeneration (Heneka et al., 2015). To investigate whether neuroinflammation is a potential mechanism of pigment

engulfment and clearance in our model, we assessed glial reactivity in the region throughout the neurodegenerative process. While we found minimal differences in microglial reactivity at 4- or 6-weeks (data not shown), we observed robust GFAP+ astrocyte reactivity in and around the LC of pigment-expressing mice at both 4- and 6-weeks, well beyond the levels seen in controls (**Fig. 7a-f**). Furthermore, there was extensive overlap between GFAP immunoreactivity and pigment, suggesting some interaction between the astrocytes and pigment granules (**Fig. 7g**).

Loss of pigment-bearing noradrenergic neurons depletes catecholamine levels in the LC and projection regions and dysregulates NE turnover.

Following pigment-mediated LC degeneration at 6 weeks post-infusion, we re-assessed tissue catecholamine levels. In line with the 1-week data, we found an even greater decrease in NE in the pons ($t_{(9)} = 10.23$, $p < 0.0001$;), PFC ($t_{(9)} = 9.745$, $p < 0.0001$), and hippocampus ($t_{(9)} = 12.83$, < 0.0001) of hTyr-injected mice as compared to EYFP controls (**Fig. 8**). Similarly, we found a decrease in MHPG in the pons ($t_{(9)} = 9.489$, $p < 0.0001$), PFC ($t_{(9)} = 7.659$, $p < 0.0001$), and hippocampus ($t_{(9)} = 8.207$, $p < 0.0001$) (**Fig. 8**). While NE turnover (MHPG:NE) was decreased in the pons ($t_{(9)} = 4.427$, $p = 0.0017$), the increased NE turnover seen in projection regions at 1 week persisted in the PFC ($t_{(9)} = 3.11$, $p = 0.0125$) and hippocampus ($t_{(9)} = 2.697$, $p = 0.0245$) at 6 weeks (**Fig. 8**). Furthermore, DA turnover was increased in the hippocampus of hTyr-injected animals ($t_{(9)} = 2.623$, $p = 0.0277$), likely driven by an increase of the metabolite DOPAC ($t_{(9)} = 3.079$, $p = 0.0132$). No changes in 5-HT, metabolite 5-HIAA, or turnover was found in any region at 6 weeks (**Table 2**).

Pigment-mediated neurodegeneration has subtle behavioral effects at 6-weeks. Despite the catastrophic loss of LC neurons and decrease in neurotransmitter levels at 6-weeks, the behavioral effects resulting from prolonged pigment expression were subtle. Pigment-expressing mice displayed no differences in sleep latency (**Fig. 9a**). Novelty-induced anxiety, which was increased in hTyr mice at 1-week, did not differ statistically between groups at 6-weeks (**Fig. 9b**). Additionally, there were no differences observed in the context fear testing assay (**Fig. 9c**).

Discussion

The present study characterized the impact of hTyr-induced pigment in the LC of mice, allowing causal relationships between NM expression in noradrenergic neurons, LC-NE integrity, and the development of non-motor symptoms reminiscent of prodromal PD in humans. The expression of pigmentation driven by viral delivery of hTyr is consistent with prior work focused on the SN (Carballo-Carbajal et al., 2019). In our model, neuronal dysfunction is evident as early as 1-week post-infusion. Even at this early time point, we found a modest decrease in the number of cell bodies present in the LC, as well as dramatically decreased NET immunoreactivity in the pons, PFC, and hippocampus of hTyr mice compared to controls. These findings are consistent with other reports of early LC axon loss in neurodegenerative diseases (Weinshenker, 2018; Doppler et al., 2021). Concurrent with fiber loss was a depletion of NE and its primary metabolite MHPG in the hippocampus and PFC. We also found elevated MHPG:NE ratio, a well validated measure of NE turnover, in projection regions, which may suggest compensatory hyperactivity of surviving LC fibers. This feature has been described in other rodent models of LC neurodegeneration (Hallman and Jonsson, 1984; Iannitelli et al., 2022) and is also consistent with LC neurodegeneration in humans (Francis et al., 1985; Raskind et al., 1999; Jacobs et al., 2021).

An overactive NE transmission phenotype would be congruent with the pre-degenerative LC dysfunction seen in humans with PD (Weinshenker, 2018). Indeed, pigment-expressing mice displayed elevated novelty-induced anxiety-like behavior and a trend towards increased latency to sleep at 1 week, indicating increased noradrenergic neurotransmission (Porter-Stransky et al., 2019; Butkovich et al., 2020; Lustberg et al., 2020c). These results were perhaps surprising given the significant loss of noradrenergic fibers and NE in projections. However, the increased NE turnover suggests that surviving fibers compensate for the loss of neighboring LC neuron terminals, and we and others have observed adrenergic receptor hypersensitivity following neurotoxic lesions of LC terminals that may also be present here (Wolfman et al., 1994; Szot et al., 2010; Iannitelli et al., 2022). Finally, increased turnover of DA in the pons and PFC at 1-week could be contributing to the anxiety-like and arousal phenotypes seen in pigment-expressing mice at this time point.

On a molecular level, we found that hTyr expression led to the upregulation of several important pathways. Isolation of LC-mRNA with TRAP yielded several hundred genes dysregulated between hTyr and EYFP controls. While many of these genes were significantly – but not robustly on a fold-change level – dysregulated on an individual level, pathway analyses revealed these subtle changes may have a concomitant impact on cellular health and functioning. Unsurprisingly, metabolism of the amino acids tyrosine and tryptophan, in addition to the metabolism of DA itself, were highly enriched in pigmented LC neurons. Similar increases were seen in macroautophagy and lysosome activity, indicating a cellular attempt to clear granules from the cytosol. Importantly, lysosomal dysfunction has been closely linked to PD (Nguyen et al., 2019). The upregulation of several additional pathways was directly linked to the production of pigment granules. These include increases in peroxisome activity (involved in oxidation), the

response to heavy metal ions iron and manganese, and in the pigment metabolic process and pigment granule formation.

Perhaps the most intriguing results from our pathway analyses were the upregulation of specific stress response systems, immune reactions, and subsequent apoptosis in pigmented neurons. Reliable increases in P53 signaling pathways were found throughout each of our analyses, indicating severe cellular stress. Endoplasmic reticulum stress was also a consistent finding in the gene ontology biological processes analysis, revealing that cellular pigment has a severe impact on the crucial function that the endoplasmic reticulum plays in calcium storage, protein synthesis and lipid metabolism. Antigen presentation via MHC-I was the most enriched pathway in all of our analyses, providing a clue about how LC neurons respond to pigment burden. The primary function of MHC-I is to present endogenous particles to signal cytotoxic T-cells, an intervention which leads to cellular destruction. Remarkably, catecholamine neurons are the only neurons known to express MHC-I (Cebrian et al., 2014), providing a tantalizing link between the unique possession of NM and a mechanism for dealing with this burden once it becomes harmful to the cell. In line with this theory, several apoptotic and cell-death-related pathways were also upregulated in our analyses. While these preliminary transcriptomic analyses are informative, further investigation into the specific genes driving these pathway changes is warranted. However, these findings provide preliminary evidence of potential links between our rodent model LC pigmentation and real PD-related symptoms seen in human patients.

Substantial cell death was visible by 6- to 8-weeks post-infusion, and was accompanied by a robust glial response. While microglia are most often associated with clearing extracellular debris, we found that the astrocyte response was dominant in our model. One potential explanation could be the timing of our histological experiments. As others have reported an early

microglial response to pigmented neurons (Carballo-Carbajal et al., 2019), it is possible that the assessment of glia several weeks post-injection represents a late or prolonged immune response, which may be dominated by astrocytes. For this reason, glial responses at the 1-week will be a critical analysis in our future investigations of this rodent model. Neuroinflammation is a well-appreciated aspect of PD (Tansey et al., 2022), and our data suggest that the presence of pigmentation in degenerating LC neurons could be contributing to the neuroimmune response.

This loss of noradrenergic neurons resulted in a decrease of NE and its metabolite in the pons itself, as well as a near-total depletion in both terminal fields assessed. NE turnover was decreased in the pons, but similar to the results obtained at 1-week, turnover was increased in the hippocampus and PFC. DA turnover was also increased in the hippocampus at the 6-week timepoint. This dysregulation may account for the subtle behavioral changes seen despite the significant loss of LC neurons at this endpoint. There were no differences between groups in sleep latency, novelty-induced anxiety, or contextual fear memory. The loss of an anxiety-like phenotype at 6-weeks may be explained by a near-total loss of LC-NE, which is required for this behavior (Lustberg et al., 2020a). While contextual fear memory should also require LC innervation of the hippocampus (McGaugh, 2013), recent studies have also implicated DA in hippocampal function and fear memory (Likhtik and Johansen, 2019; Stubbendorff and Stevenson, 2021). Thus, the increase in DA turnover in the hippocampus at 6-weeks may account for the lack of behavioral differences seen in the contextual fear task.

The present study describes the first analysis of pigment induction in the rodent LC, providing critical insight into the consequences of granule accumulation in noradrenergic neurons. We found that pigment expression dysregulates LC neurons on a cellular and molecular level at 1 week, triggering phenotypes reminiscent of non-motor symptoms in prodromal PD. As

the pigment accumulates, immune response and neurodegeneration ensue. By 6-weeks post-infusion, the LC has nearly entirely degenerated, having detrimental effects on neurotransmission but not on mouse behavior. Future work should focus on a mid-point which represents moderate neurodegeneration, as well as a later endpoint representing a total loss of LC neurons. Furthermore, pigment-mediated changes in noradrenergic and dopaminergic neurons should be compared to assess the differences in responding and rate of cell death between LC-NM and SN-NM. Indeed, it was reported that hTyr-expressing SN-DA neurons took many months to degenerate (Carballo-Carbajal et al., 2019). It is not clear whether this reflects differences with our model in the virus itself (AAV2 vs Cre-dependent AAV5), species (rat vs mouse), or a true greater vulnerability of LC neurons. Thus, direct comparisons using the same lot of virus in parallel will be needed. Ultimately, this model of pigment induction in rodent catecholamine neurons may be critical for uncovering the role NM plays in PD onset and progression.

Author Contributions

A.F.I. designed and performed research, analyzed data, and wrote the manuscript. A.S. performed research and analyzed data. J. F. P. performed research and analyzed data. B.M. assisted with research design and data analysis. L.C.L. assisted with research design and analysis. S.A.S. assisted with research design and data analysis. K.E.M. performed research and analyzed data. J.D.D. assisted with research design and contributed analytic tools. Y.S. assisted with research design and data analysis. D.W. designed research and assisted in writing the manuscript.

Acknowledgements

This work was supported by a National Institutes of Health (NIH) National Institute of Environmental Health Sciences Training Grant (ES12870) and a NIH D-SPAN F99/K00 Award from the National Institute of Neurological Disorders and Stroke (NS129168) to A.F.I, as well as RF1 awards from the National Institute on Aging (AG079199 and AG061175) to D.W. This study was supported in part by the Emory HPLC Bioanalytical Core (EHBC), which is subsidized by the Emory University School of Medicine and is one of the Emory Integrated Core Facilities. Additional support was provided by the Georgia Clinical & Translational Science Alliance of the National Institutes of Health under Award Number UL1TR002378. We thank Dr. M. McGuirk Sampson for assistance with R code for analysis.

References

Barden H, Levine S (1983) Histochemical observations on rodent brain melanin. Brain Res Bull 10:847-851.

Bush WD, Garguilo J, Zucca FA, Albertini A, Zecca L, Edwards GS, Nemanich RJ, Simon JD (2006) The surface oxidation potential of human neuromelanin reveals a spherical architecture with a pheomelanin core and a eumelanin surface. Proc Natl Acad Sci U S A 103:14785-14789.

Butkovich LM, Houser MC, Chalermpalanupap T, Porter-Stransky KA, Iannitelli AF, Boles JS, Lloyd GM, Coomes AS, Eidson LN, De Sousa Rodrigues ME, Oliver DL, Kelly SD, Chang J, Bengoa-Vergniory N, Wade-Martins R, Giasson BI, Joers V, Weinshenker D, Tansey MG (2020) Transgenic Mice Expressing Human alpha-Synuclein in Noradrenergic Neurons Develop Locus Ceruleus Pathology and Nonmotor Features of Parkinson's Disease. J Neurosci 40:7559-7576.

Carballo-Carbajal I, Laguna A, Romero-Gimenez J, Cuadros T, Bove J, Martinez-Vicente M, Parent A, Gonzalez-Sepulveda M, Penuelas N, Torra A, Rodriguez-Galvan B, Ballabio A, Hasegawa T, Bortolozzi A, Gelpi E, Vila M (2019) Brain tyrosinase overexpression implicates age-dependent neuromelanin production in Parkinson's disease pathogenesis. Nat Commun 10:973.

Cebrian C, Zucca FA, Mauri P, Steinbeck JA, Studer L, Scherzer CR, Kanter E, Budhu S, Mandelbaum J, Vonsattel JP, Zecca L, Loike JD, Sulzer D (2014) MHC-I expression renders catecholaminergic neurons susceptible to T-cell-mediated degeneration. Nat Commun 5:3633.

Chalermpalanupap T, Schroeder JP, Rorabaugh JM, Liles LC, Lah JJ, Levey AI, Weinshenker D (2018) Locus Coeruleus Ablation Exacerbates Cognitive Deficits, Neuropathology, and Lethality in P301S Tau Transgenic Mice. J Neurosci 38:74-92.

Chan-Palay V (1991) Alterations in the locus coeruleus in dementias of Alzheimer's and Parkinson's disease. Prog Brain Res 88:625-630.

Del Tredici K, Braak H (2013) Dysfunction of the locus coeruleus-norepinephrine system and related circuitry in Parkinson's disease-related dementia. J Neurol Neurosurg Psychiatry 84:774-783.

DeMattei M, Levi AC, Fariello RG (1986) Neuromelanic pigment in substantia nigra neurons of rats and dogs. Neurosci Lett 72:37-42.

Dexter DT, Jenner P, Schapira AH, Marsden CD (1992) Alterations in levels of iron, ferritin, and other trace metals in neurodegenerative diseases affecting the basal ganglia. The Royal Kings and Queens Parkinson's Disease Research Group. Ann Neurol 32 Suppl:S94-100.

Doppler CEJ, Kinnerup MB, Brune C, Farrher E, Betts M, Fedorova TD, Schaldemose JL, Knudsen K, Ismail R, Seger AD, Hansen AK, Staer K, Fink GR, Brooks DJ, Nahimi A, Borghammer P, Sommerauer M (2021) Regional locus coeruleus degeneration is uncoupled from noradrenergic terminal loss in Parkinson's disease. Brain.

Foote SL, Bloom FE, Aston-Jones G (1983) Nucleus locus ceruleus: new evidence of anatomical and physiological specificity. Physiol Rev 63:844-914.

Francis PT, Palmer AM, Sims NR, Bowen DM, Davison AN, Esiri MM, Neary D, Snowden JS, Wilcock GK (1985) Neurochemical studies of early-onset Alzheimer's disease. Possible influence on treatment. N Engl J Med 313:7-11.

Hallman H, Jonsson G (1984) Monoamine neurotransmitter metabolism in microencephalic rat brain after prenatal methylazoxymethanol treatment. Brain Res Bull 13:383-389.

Heneka MT et al. (2015) Neuroinflammation in Alzheimer's disease. Lancet Neurol 14:388-405.
Hinson VK, Delambo A, Elm J, Turner T (2017) A Randomized Clinical Trial of Atomoxetine for Mild Cognitive Impairment in Parkinson's Disease. Mov Disord Clin Pract 4:416-423.
Hunsley MS, Palmiter RD (2004) Altered sleep latency and arousal regulation in mice lacking norepinephrine. Pharmacol Biochem Behav 78:765-773.
Iannitelli AF, Kelberman MA, Lustberg DJ, Korukonda A, McCann KE, Mulvey B, Segal A, Liles LC, Sloan SA, Dougherty JD, Weinshenker D (2022) The Neurotoxin DSP-4 Dysregulates the Locus Coeruleus-Norepinephrine System and Recapitulates Molecular and Behavioral Aspects of Prodromal Neurodegenerative Disease. bioRxiv:2022.2009.2027.509797.
Jacobs HIL, Becker JA, Kwong K, Engels-Dominguez N, Prokopiou PC, Papp KV, Properzi M, Hampton OL, d'Oleire Uquillas F, Sanchez JS, Rentz DM, El Fakhri G, Normandin MD, Price JC, Bennett DA, Sperling RA, Johnson KA (2021) In vivo and neuropathology data support locus coeruleus integrity as indicator of Alzheimer's disease pathology and cognitive decline. Sci Transl Med 13:eabj2511.
Kang SS, Liu X, Ahn EH, Xiang J, Manfredsson FP, Yang X, Luo HR, Liles LC, Weinshenker D, Ye K (2020) Norepinephrine metabolite DOPEGAL activates AEP and pathological Tau aggregation in locus coeruleus. J Clin Invest 130:422-437.
Li Y, Wang C, Wang J, Zhou Y, Ye F, Zhang Y, Cheng X, Huang Z, Liu K, Fei G, Zhong C, Zeng M, Jin L (2019) Mild cognitive impairment in de novo Parkinson's disease: A neuromelanin MRI study in locus coeruleus. Mov Disord 34:884-892.
Likhtik E, Johansen JP (2019) Neuromodulation in circuits of aversive emotional learning. Nat Neurosci 22:1586-1597.
Lustberg D, Iannitelli AF, Tillage RP, Pruitt M, Liles LC, Weinshenker D (2020a) Central norepinephrine transmission is required for stress-induced repetitive behavior in two rodent models of obsessive-compulsive disorder. Psychopharmacology (Berl) 237:1973-1987.
Lustberg D, Iannitelli AF, Tillage RP, Pruitt M, Liles LC, Weinshenker D (2020b) Central norepinephrine transmission is required for stress-induced repetitive behavior in two rodent models of obsessive-compulsive disorder. Psychopharmacology (Berl).
Lustberg D, Tillage RP, Bai Y, Pruitt M, Liles LC, Weinshenker D (2020c) Noradrenergic circuits in the forebrain control affective responses to novelty. Psychopharmacology (Berl) 237:3337-3355.
Lustberg DJ, Liu JQ, Iannitelli AF, Vanderhoof SO, Liles LC, McCann KE, Weinshenker D (2022) Norepinephrine and dopamine contribute to distinct repetitive behaviors induced by novel odorant stress in male and female mice. Horm Behav 144:105205.
Mann DM, Yates PO (1974) Lipoprotein pigments--their relationship to ageing in the human nervous system. II. The melanin content of pigmented nerve cells. Brain 97:489-498.
Mann DM, Yates PO (1983) Possible role of neuromelanin in the pathogenesis of Parkinson's disease. Mech Ageing Dev 21:193-203.
Marras C, Beck JC, Bower JH, Roberts E, Ritz B, Ross GW, Abbott RD, Savica R, Van Den Eeden SK, Willis AW, Tanner CM, Parkinson's Foundation PG (2018) Prevalence of Parkinson's disease across North America. NPJ Parkinsons Dis 4:21.
Mavridis M, Degryse AD, Lategan AJ, Marien MR, Colpaert FC (1991) Effects of locus coeruleus lesions on parkinsonian signs, striatal dopamine and substantia nigra cell loss

after 1-methyl-4-phenyl-1,2,3,6-tetrahydropyridine in monkeys: a possible role for the locus coeruleus in the progression of Parkinson's disease. Neuroscience 41:507-523.
McGaugh JL (2013) Making lasting memories: remembering the significant. Proc Natl Acad Sci U S A 110 Suppl 2:10402-10407.
Mootha VK et al. (2003) PGC-1alpha-responsive genes involved in oxidative phosphorylation are coordinately downregulated in human diabetes. Nat Genet 34:267-273.
Mulvey B, Bhatti DL, Gyawali S, Lake AM, Kriaucionis S, Ford CP, Bruchas MR, Heintz N, Dougherty JD (2018) Molecular and Functional Sex Differences of Noradrenergic Neurons in the Mouse Locus Coeruleus. Cell Rep 23:2225-2235.
Murchison CF, Zhang XY, Zhang WP, Ouyang M, Lee A, Thomas SA (2004) A distinct role for norepinephrine in memory retrieval. Cell 117:131-143.
Nguyen M, Wong YC, Ysselstein D, Severino A, Krainc D (2019) Synaptic, Mitochondrial, and Lysosomal Dysfunction in Parkinson's Disease. Trends Neurosci 42:140-149.
Nicholls DG (2008) Oxidative stress and energy crises in neuronal dysfunction. Ann N Y Acad Sci 1147:53-60.
Pall HS, Williams AC, Blake DR, Lunec J, Gutteridge JM, Hall M, Taylor A (1987) Raised cerebrospinal-fluid copper concentration in Parkinson's disease. Lancet 2:238-241.
Porter-Stransky KA, Centanni SW, Karne SL, Odil LM, Fekir S, Wong JC, Jerome C, Mitchell HA, Escayg A, Pedersen NP, Winder DG, Mitrano DA, Weinshenker D (2019) Noradrenergic Transmission at Alpha1-Adrenergic Receptors in the Ventral Periaqueductal Gray Modulates Arousal. Biol Psychiatry 85:237-247.
Prediger RD, Matheus FC, Schwarzbold ML, Lima MM, Vital MA (2012) Anxiety in Parkinson's disease: a critical review of experimental and clinical studies. Neuropharmacology 62:115-124.
Raskind MA, Peskind ER, Holmes C, Goldstein DS (1999) Patterns of cerebrospinal fluid catechols support increased central noradrenergic responsiveness in aging and Alzheimer's disease. Biol Psychiatry 46:756-765.
Remy P, Doder M, Lees A, Turjanski N, Brooks D (2005) Depression in Parkinson's disease: loss of dopamine and noradrenaline innervation in the limbic system. Brain 128:1314-1322.
Sanchez-Padilla J, Guzman JN, Ilijic E, Kondapalli J, Galtieri DJ, Yang B, Schieber S, Oertel W, Wokosin D, Schumacker PT, Surmeier DJ (2014) Mitochondrial oxidant stress in locus coeruleus is regulated by activity and nitric oxide synthase. Nat Neurosci 17:832-840.
Sasaki M, Shibata E, Tohyama K, Takahashi J, Otsuka K, Tsuchiya K, Takahashi S, Ehara S, Terayama Y, Sakai A (2006) Neuromelanin magnetic resonance imaging of locus ceruleus and substantia nigra in Parkinson's disease. Neuroreport 17:1215-1218.
Song S, Wang Q, Jiang L, Oyarzabal E, Riddick NV, Wilson B, Moy SS, Shih YI, Hong JS (2019) Noradrenergic dysfunction accelerates LPS-elicited inflammation-related ascending sequential neurodegeneration and deficits in non-motor/motor functions. Brain Behav Immun 81:374-387.
Srinivasan J, Schmidt WJ (2003) Potentiation of parkinsonian symptoms by depletion of locus coeruleus noradrenaline in 6-hydroxydopamine-induced partial degeneration of substantia nigra in rats. Eur J Neurosci 17:2586-2592.
Stiasny-Kolster K, Doerr Y, Moller JC, Hoffken H, Behr TM, Oertel WH, Mayer G (2005) Combination of 'idiopathic' REM sleep behaviour disorder and olfactory dysfunction as

possible indicator for alpha-synucleinopathy demonstrated by dopamine transporter FP-CIT-SPECT. Brain 128:126-137.
Stubbendorff C, Stevenson CW (2021) Dopamine regulation of contextual fear and associated neural circuit function. Eur J Neurosci 54:6933-6947.
Subramanian A, Tamayo P, Mootha VK, Mukherjee S, Ebert BL, Gillette MA, Paulovich A, Pomeroy SL, Golub TR, Lander ES, Mesirov JP (2005) Gene set enrichment analysis: a knowledge-based approach for interpreting genome-wide expression profiles. Proc Natl Acad Sci U S A 102:15545-15550.
Sulzer D, Mosharov E, Talloczy Z, Zucca FA, Simon JD, Zecca L (2008) Neuronal pigmented autophagic vacuoles: lipofuscin, neuromelanin, and ceroid as macroautophagic responses during aging and disease. J Neurochem 106:24-36.
Sulzer D, Bogulavsky J, Larsen KE, Behr G, Karatekin E, Kleinman MH, Turro N, Krantz D, Edwards RH, Greene LA, Zecca L (2000) Neuromelanin biosynthesis is driven by excess cytosolic catecholamines not accumulated by synaptic vesicles. Proc Natl Acad Sci U S A 97:11869-11874.
Surmeier DJ, Guzman JN, Sanchez-Padilla J (2010) Calcium, cellular aging, and selective neuronal vulnerability in Parkinson's disease. Cell Calcium 47:175-182.
Szot P, Miguelez C, White SS, Franklin A, Sikkema C, Wilkinson CW, Ugedo L, Raskind MA (2010) A comprehensive analysis of the effect of DSP4 on the locus coeruleus noradrenergic system in the rat. Neuroscience 166:279-291.
Tansey MG, Wallings RL, Houser MC, Herrick MK, Keating CE, Joers V (2022) Inflammation and immune dysfunction in Parkinson disease. Nat Rev Immunol.
Tillage RP, Wilson GE, Liles LC, Holmes PV, Weinshenker D (2020a) Chronic Environmental or Genetic Elevation of Galanin in Noradrenergic Neurons Confers Stress Resilience in Mice. J Neurosci 40:7464-7474.
Tillage RP, Sciolino NR, Plummer NW, Lustberg D, Liles LC, Hsiang M, Powell JM, Smith KG, Jensen P, Weinshenker D (2020b) Elimination of galanin synthesis in noradrenergic neurons reduces galanin in select brain areas and promotes active coping behaviors. Brain Struct Funct 225:785-803.
Vazey EM, Aston-Jones G (2012) The emerging role of norepinephrine in cognitive dysfunctions of Parkinson's disease. Front Behav Neurosci 6:48.
Wang X, Michaelis EK (2010) Selective neuronal vulnerability to oxidative stress in the brain. Front Aging Neurosci 2:12.
Weinshenker D (2018) Long Road to Ruin: Noradrenergic Dysfunction in Neurodegenerative Disease. Trends Neurosci 41:211-223.
Wolfman C, Abo V, Calvo D, Medina J, Dajas F, Silveira R (1994) Recovery of central noradrenergic neurons one year after the administration of the neurotoxin DSP4. Neurochem Int 25:395-400.
Zecca L, Zucca FA, Wilms H, Sulzer D (2003) Neuromelanin of the substantia nigra: a neuronal black hole with protective and toxic characteristics. Trends Neurosci 26:578-580.
Zecca L, Wilms H, Geick S, Claasen JH, Brandenburg LO, Holzknecht C, Panizza ML, Zucca FA, Deuschl G, Sievers J, Lucius R (2008a) Human neuromelanin induces neuroinflammation and neurodegeneration in the rat substantia nigra: implications for Parkinson's disease. Acta Neuropathol 116:47-55.
Zecca L, Stroppolo A, Gatti A, Tampellini D, Toscani M, Gallorini M, Giaveri G, Arosio P, Santambrogio P, Fariello RG, Karatekin E, Kleinman MH, Turro N, Hornykiewicz O,

Zucca FA (2004) The role of iron and copper molecules in the neuronal vulnerability of locus coeruleus and substantia nigra during aging. Proc Natl Acad Sci U S A 101:9843-9848.

Zecca L, Bellei C, Costi P, Albertini A, Monzani E, Casella L, Gallorini M, Bergamaschi L, Moscatelli A, Turro NJ, Eisner M, Crippa PR, Ito S, Wakamatsu K, Bush WD, Ward WC, Simon JD, Zucca FA (2008b) New melanic pigments in the human brain that accumulate in aging and block environmental toxic metals. Proc Natl Acad Sci U S A 105:17567-17572.

Zweig RM, Cardillo JE, Cohen M, Giere S, Hedreen JC (1993) The locus ceruleus and dementia in Parkinson's disease. Neurology 43:986-991.

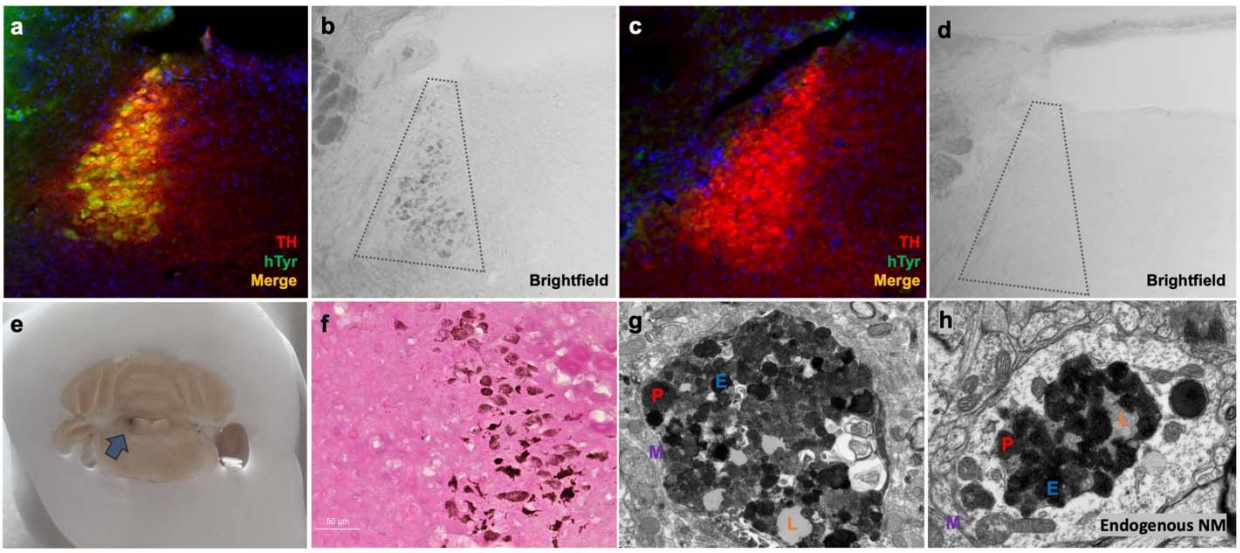

Fig. 1. hTyr induces pigmentation in the LC reminiscent of endogenous NM. Mice received stereotaxic injection of AAV5-DIO-hTyr into the LC, driving expression of human Tyrosinase in TH-Cre+ experimental animals (**a**) but not in TH-Cre- controls (**c**). Although rodents (TH-Cre- image shown here) do not display endogenous NM (**d**), the presence of hTyr resulted in LC pigmentation visible by brightfield microscopy (**b**) and gross anatomical inspection (arrow) (**e**). This hTyr-derived pigment stained positive for melanin components with Fontana-Masson (**f**), and electron microscopic analysis of these granules (**g**) showed they contain several features characteristic of endogenous NM from aged rhesus macaques (**h**), including pheomelanin (P, red), eumelanin (E, blue), lipid droplets (L, orange), and enclosure in a membrane (M, purple). Immunofluorescent and brightfield images (A-D, F) were acquired at 20x magnification.

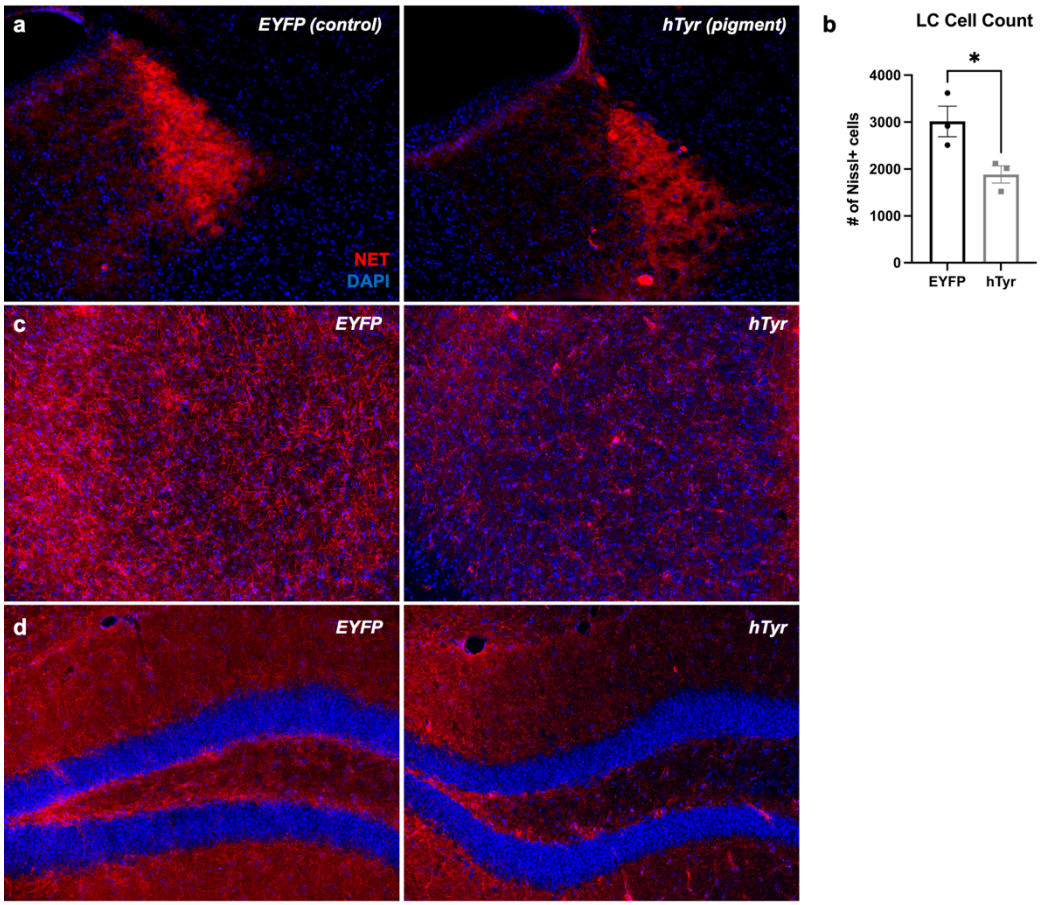

Fig. 2. The presence of NM-like pigmentation damages LC cell bodies and fibers at 1-week. TH-Cre mice received LC infusion of AAV5-DIO-hTyr or EYFP control and were assessed for locus coeruleus (LC) neuron damage 1 week later. hTyr-induced pigment expression resulted in substantial loss of axon terminals as measured by norepinephrine transporter (NET) immunoreactivity in the dentate gyrus (DG) (**d**) and anterior cingulate cortex (ACC) (**c**), with a similar decrease in NET also present in the LC itself (**a**). Concurrent with NE fiber loss was a decrease in LC cell body number as measured by NeuroTrace Nissl immunoreactivity (**b**). Images acquired at 20X. Data shown as mean ± SEM. N=3 per group. **p<0.01, ***p<0.001, ****p<0.0001.

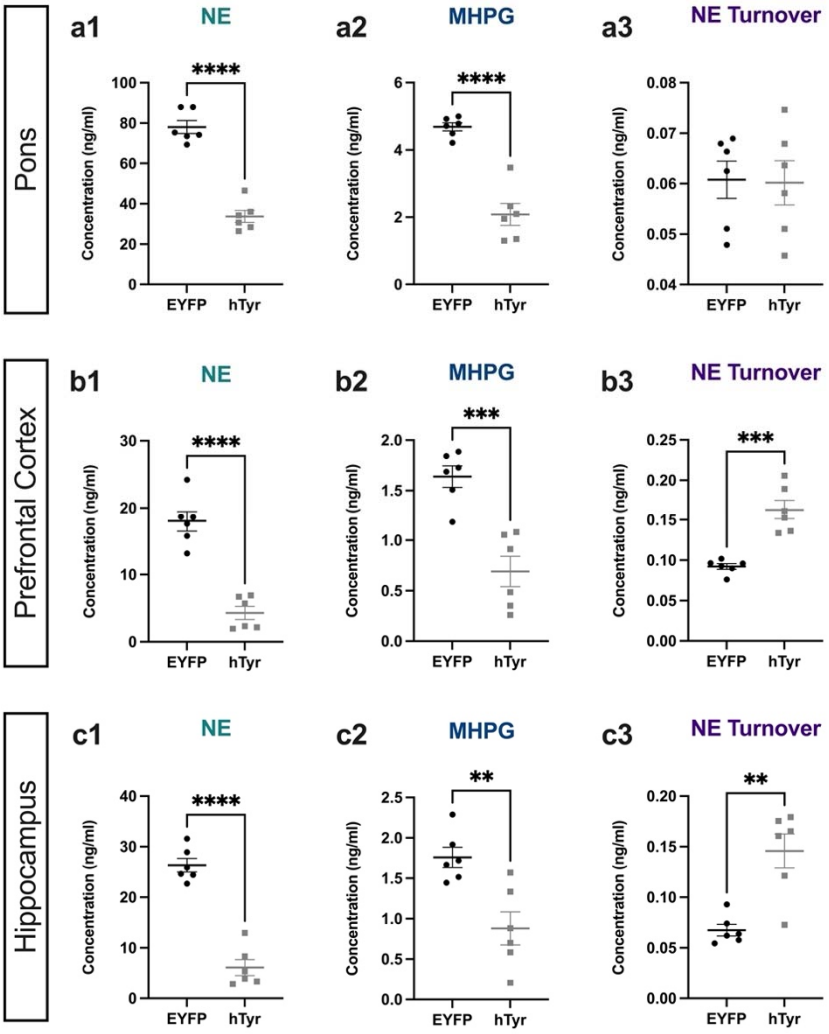

Fig. 3. hTyr-induced pigmentation decreases tissue NE and metabolite levels and increases turnover at 1 week. TH-Cre mice received stereotaxic infusion of AAV-DIO-hTyr or EYFP control into the LC, and tissue monoamine and metabolite levels were measured 1 week later by HPLC in the pons, prefrontal cortex (PFC), and hippocampus. hTyr significantly decreased NE and its primary metabolite MHPG in the pons (**a1-2**), PFC (**b1-2**), and hippocampus (**c1-2**). NE turnover, defined as the MHPG:NE ratio, was increased in PFC (**b3**) and hippocampus (**c3**). Data shown as mean ± SEM. N=6 per group. *p<0.05, **p<0.01, ****p<0.0001.

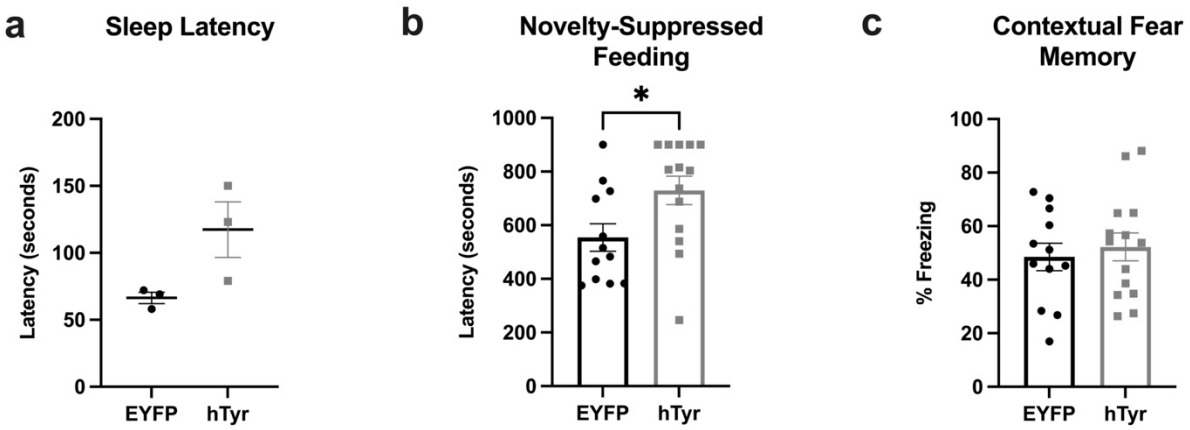

Fig. 4. hTyr-induced pigmentation increases novelty-induced anxiety but not contextual fear memory at 1 week. TH-Cre mice received stereotaxic infusion of AAV-DIO-hTyr or EYFP control into the LC, and behavior was assessed 1 week later. hTyr-expressing mice displayed a trend towards increased latency to sleep in their home cage following gentle handling (**a**), increased latency to bite the food pellet in the novelty-suppressed feeding test (**b**), but no difference in freezing behavior in the contextual conditioning fear assay (**c**) (N=12-14 per group).

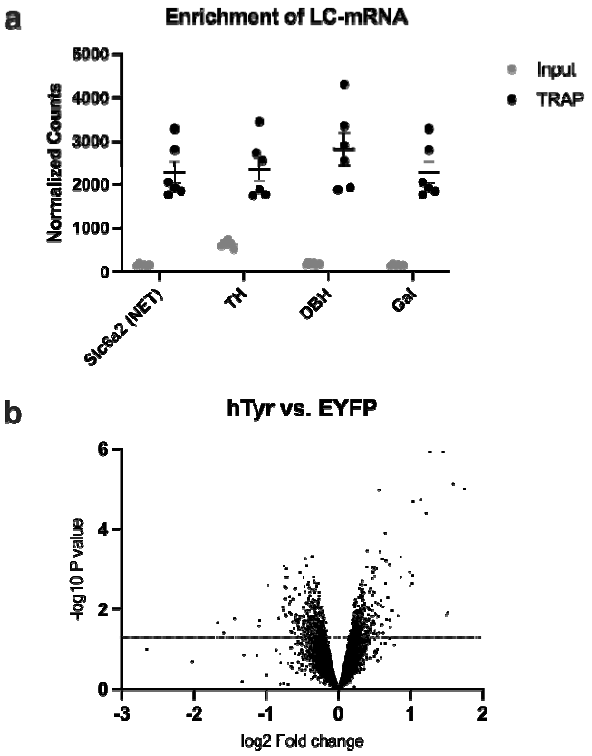

c

GeneSet	Pathway	Enrichment Score	p-value
KEGG	Tyrosine metabolism	0.62	0.008
KEGG	Tryptophan metabolism	0.60	0.014
KEGG	P53 signaling	0.51	0.018
KEGG	Adhesion molecules	0.41	0.030
KEGG	Melanoma	0.41	0.067
KEGG	Peroxisome	0.37	0.058
KEGG	Lysosome	0.35	0.042
KEGG	Calcium signaling	-0.43	0.010
KEGG	Oxidative phosphorylation	-0.41	0.032
KEGG	Alzheimer's disease	-0.37	0.075
HPO	Parkinsonism	0.54	0.039
HPO	Exaggerated startle response	0.56	0.047
HPO	Speech articulation	0.58	0.040
HPO	Sleep apnea	0.59	0.021
HPO	Delusions	-0.62	0.003
GO:BP	Regulation of extrinsic apoptotic signaling pathway	0.70	0.000
GO:BP	Antigen processing and presentation via MHC-I	0.74	0.000
GO:BP	Response to iron ion	0.61	0.018
GO:BP	Positive regulation of T-cell mediated immunity	0.61	0.027
GO:BP	Response to manganese ion	0.57	0.047
GO:BP	Dopamine metabolic process	0.49	0.047
GO:BP	Positive regulation of macroautophagy	0.47	0.011
GO:BP	Pigment metabolic process	0.46	0.024
GO:BP	Response to endoplasmic reticulum stress	0.42	0.00
GO:BP	Neuron death	0.30	0.011
GO:CC	Pigment granule	0.43	0.00

Fig. 5. hTyr-driven pigmentation triggers changes in the LC transcriptome. TH-Cre; Slc6a2-eGFP/Rpl10a mice received viral infusion of AAV5-DIO-hTyr or EYFP control in the LC, and gene expression was assessed 1 week later. We confirmed LC-mRNA enrichment in TRAP samples over hindbrain input, and found elevated levels of noradrenergic genes in the immunoprecipitated TRAP samples (**a**). Volcano plot of all filtered, normalized genes (~11,500) displaying spread of up- and down-regulated genes (**b**). Table highlighting significantly enriched KEGG, Human Phenotype Ontology (HPO), Gene Ontology Biological Process (GO:BP) and Gene Ontology Cellular Component (GO:CC) pathways of interest in our LC data (**c**).

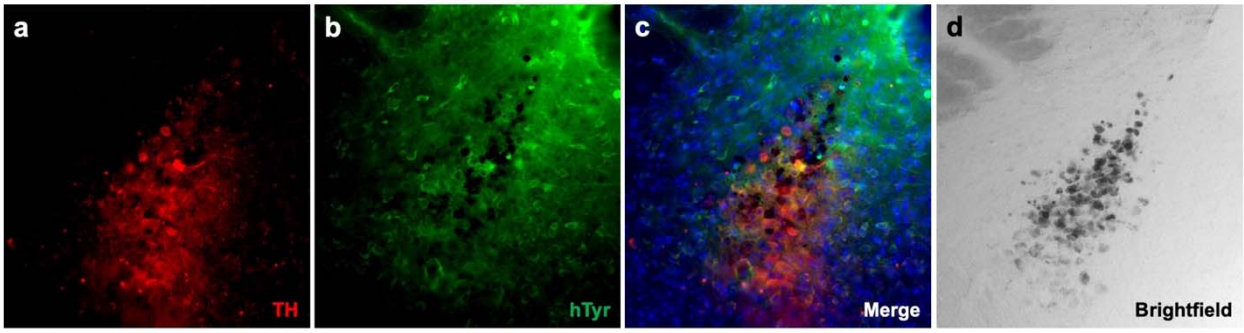

Fig. 6. Prolonged pigment expression results in granule accumulation and LC degeneration. TH-Cre mice received stereotaxic infusion of AAV-DIO-hTyr into the LC and aged for 8 weeks prior to tissue extraction and immunohistochemical assessment of LC integrity with noradrenergic marker tyrosine hydroxylase (TH) (**a**). Although expression of hTyr has diminished by 8-weeks post-injection, presumably due to loss of LC cell bodies (**b**), pigmentation remains robust in the region (**d**). Images were acquired at 20X magnification.

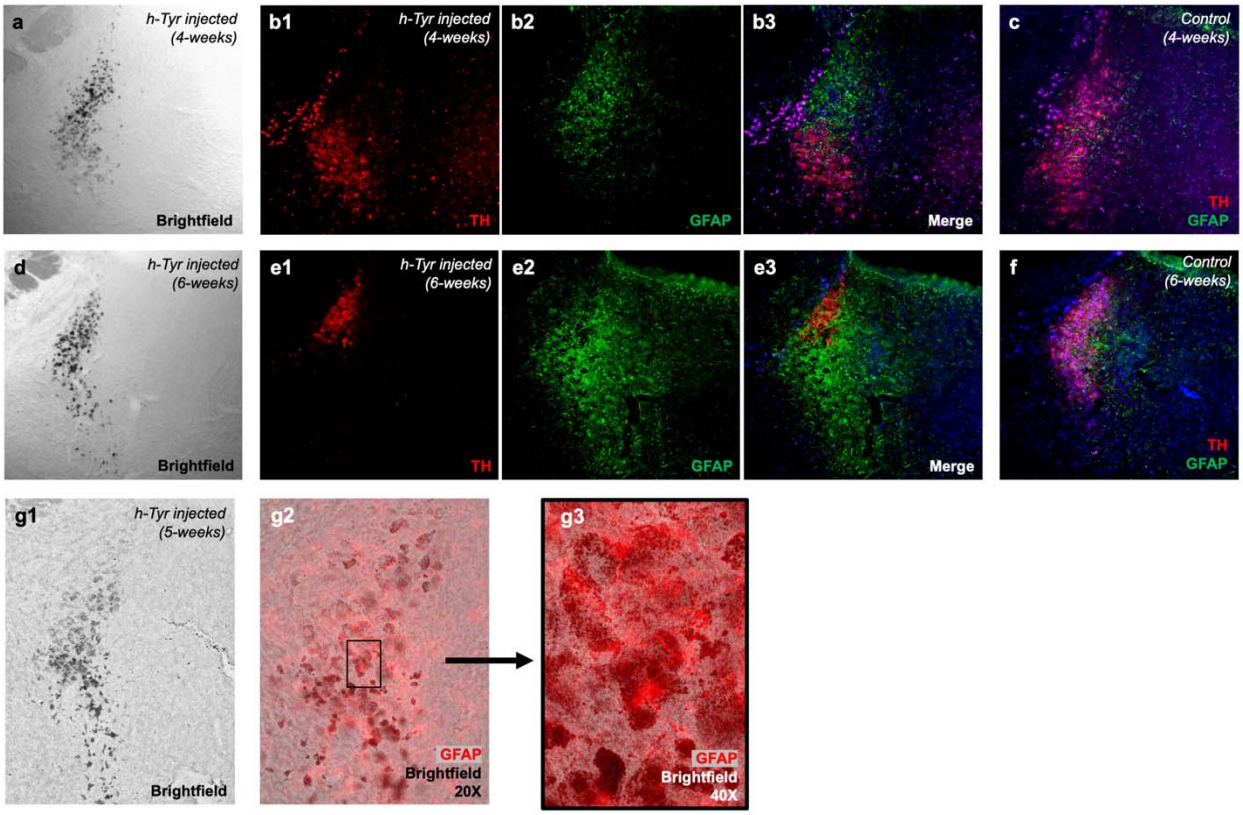

Fig. 7. Pigment-induced neurodegeneration triggers astrocyte responses in and around the LC. TH-Cre mice received AAV5-DIO-hTyr, and tissue was assessed for neuroinflammation as a result of pigment accumulation at 4-6 weeks. Over time, hTyr-induced pigmentation accumulated and darkened in the LC (**a**). Representative images show that astrocyte reactivity, as measured by GFAP immunostaining, was appreciably increased in and around the LC of hTyr-injected (**b**), but not non-expressing control mice (**c**). This process was exacerbated over time, with pigmentation becoming even more robust by 6-weeks (**d**) despite the near-total loss of TH-positive neurons (**e1**). LC neurodegeneration was accompanied by glial scarring of the region (**e**) that is not seen in non-expressing controls (**f**). Overlaying brightfield and fluorescent micrographs of the region revealed some overlap between astrocytes and pigment granules (**g**).

Images were acquired at 20X magnification, with the exception of Fig. g3, which was acquired at 40X magnification.

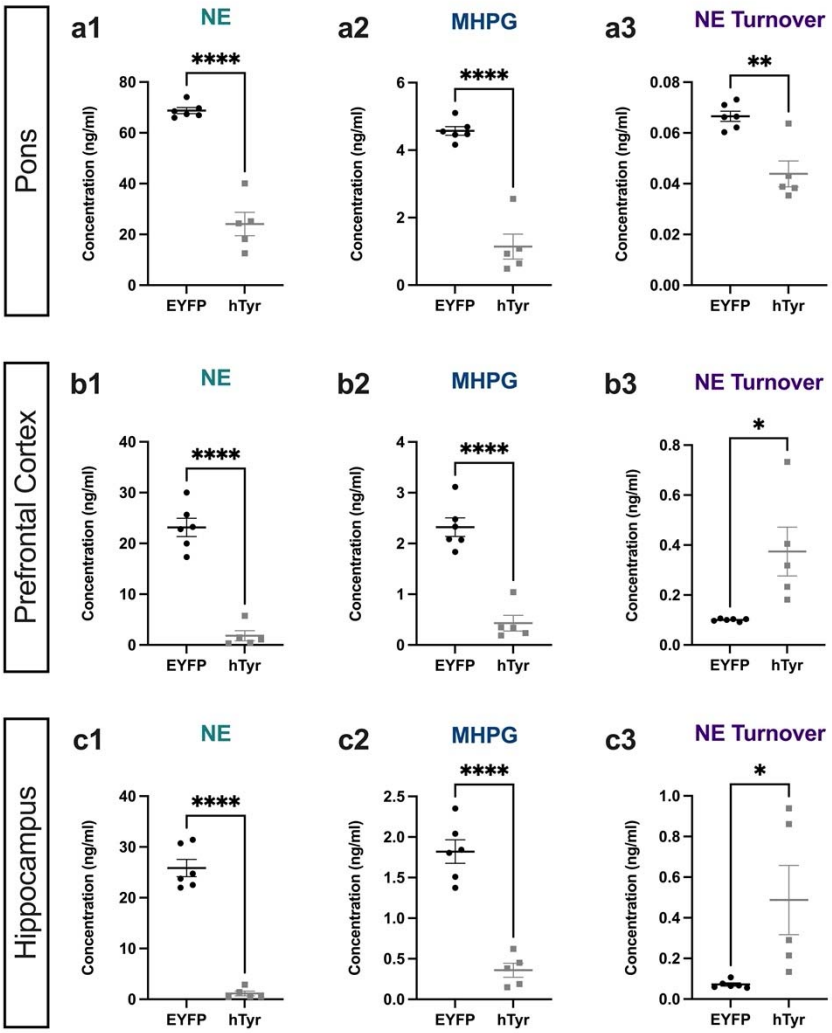

Fig. 8. hTyr-induced pigmentation depletes tissue NE and metabolite levels and dysregulates turnover at 6 weeks. TH-Cre mice received stereotaxic infusion of AAV5-DIO-hTyr or EYFP control into the LC, and tissue monoamine and metabolite levels were measured 6 weeks later by HPLC in the pons, prefrontal cortex (PFC), and hippocampus. hTyr significantly and robustly decreased NE and metabolite MHPG in the pons (**a1-2**), PFC (**b1-2**), and hippocampus (**c1-2**). NE turnover (MHPG:NE ratio) was decreased in the pons (**a3**), but

decreased in the PFC (**b3**) and hippocampus (**c3**). Data shown as mean ± SEM. N=8 per group. *p<0.05, **p<0.01, ****p<0.0001.

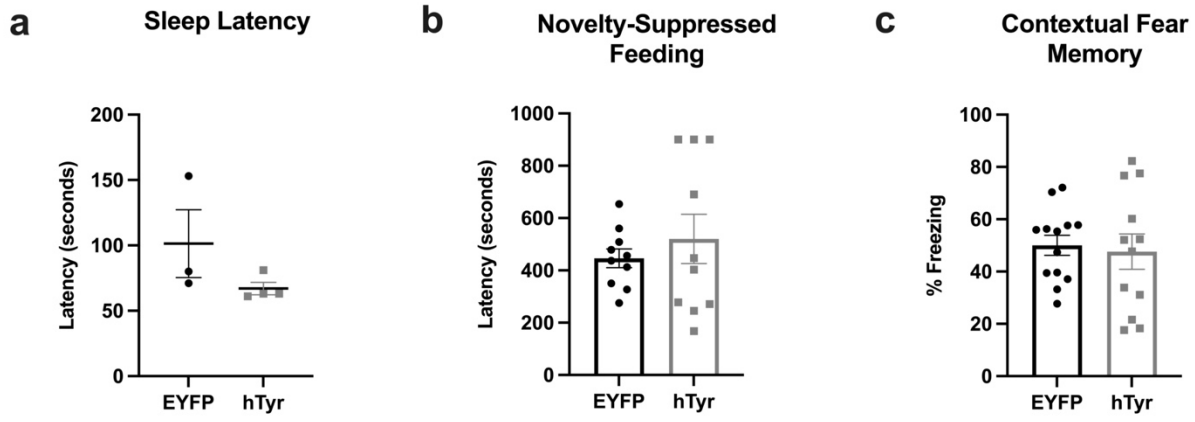

Fig. 9. Pigment accumulation and subsequent neurodegeneration does not affect novelty-induced anxiety or contextual fear memory by 6-weeks. TH-Cre mice received stereotaxic infusion of AAV5-DIO-hTyr or EYFP control into the LC, and behavior was assessed 6 weeks later. hTyr-expressing mice displayed no difference in latency to sleep (**a**), latency to bite the food pellet in the novelty-suppressed feeding test at 6-week post-infusion (**b**), and no difference in freezing behavior in the contextual fear assay (**c**) (N=12-14 per group).

Table 1. IHC antibodies

Antibodies	Host	Manufacturer	Catalog #	Dilution
Tyrosine hydroxylase	Chicken	Abcam	ab76442	1:1000
Norepinephrine transporter	Mouse	Mab Technologies	NET05-2	1:1000
Human tyrosinase	Mouse	Thermo Fisher Scientific	MS-800-B1	1:500
GFAP	Guinea Pig	Synaptic Systems	173 004	1:1000
NeuroTrace 435/455 Blue Fluorescent Nissl Stain	NA	Thermo Fisher Scientific	N21479	1:500
Alexa Fluor 488 Anti-Rabbit	Goat	Thermo Fisher Scientific	A-11008	1:500
Alexa Fluor 488 Anti-Guinea Pig	Goat	Thermo Fisher Scientific	A-11073	1:500
Alexa Fluor 568 Anti-Chicken	Goat	Thermo Fisher Scientific	A-11041	1:500

Table 2. Monoamine levels measured by HPLC

A) 1-week post-infusion

	Pons		PFC		Hippocampus	
	EYFP	**hTyr**	**EYFP**	**hTyr**	**EYFP**	**hTyr**
DA	11.37 ± 0.69	10.39 ± 0.91	20.14 ± 8.32	4.54 ± 0.38	3.53 ± 1.29	2.33 ± 0.28
DOPAC	6.98 ± 0.49	7.53 ± 0.72	3.08 ± 0.61	2.40 ± 0.20	2.52 ± 0.26	2.47 ± 0.45
DOPAC:DA	0.62 ± 0.03	0.72 ± 0.02	0.30 ± 0.08	0.53 ± 0.02	1.04 ± 0.20	1.11 ± 0.19
5-HT	170.9 ± 3.38	162.5 ± 4.33	40.66 ± 3.34	45.30 ± 2.94	69.17 ± 3.43	63.04 ± 3.73
5-HIAA	58.31 ± 3.09	61.95 ± 4.11	7.72 ± 0.22	8.59 ± 0.45	7.72 ± 0.22	8.59 ± 0.45
5-HIAA:5-HT	0.34 ± 0.02	0.38 ± 0.20	0.20 ± 0.02	0.19 ± 0.01	0.36 ± 0.03	0.38 ± 0.01

B) 6-weeks post-infusion

	Pons		PFC		Hippocampus	
	EYFP	**hTyr**	**EYFP**	**hTyr**	**EYFP**	**hTyr**
DA	9.14 ± 0.90	7.33 ± 1.06	43.34 ± 22.50	30.36 ± 16.71	2.54 ± 0.61	1.99 ± 0.37
DOPAC	6.34 ± 0.49	5.39 ± 0.70	6.33 ± 1.99	5.22 ± 1.31	1.75 ± 0.18	2.74 ± 0.28
DOPAC:DA	0.71 ± 0.05	0.75 ± 0.08	0.30 ± 0.06	0.28 ± 0.07	0.84 ± 0.16	1.53 ± 0.22
5-HT	162.6 ± 6.20	146.7 ± 4.90	62.40 ± 5.61	57.03 ± 3.27	71.83 ± 3.84	71.54 ± 3.64
5-HIAA	71.80 ± 5.58	50.41 ± 1.68	13.65 ± 2.19	10.02 ± 0.27	31.89 ± 2.02	23.78 ± 0.78
5-HIAA:5-HT	0.44 ± 0.02	0.35 ± 0.02	0.21 ± 0.01	0.18 ± 0.01	0.45 ± 0.02	0.34 ± 0.03

Data shown as mean ± SEM. N=5-6 per group. *$p<0.05$, **$p<0.01$.